Heliyon 8 (2022) e09942

Contents lists available at ScienceDirect

Heliyon

journal homepage: www.cell.com/heliyon

Research article

Porous NH_2-MIL-101(Fe) metal organic framework for effective photocatalytic degradation of azo dye in wastewater treatment

Xuezhong Li [a], Yue Wang [b,*], Qi Guo [c]

[a] School of Mechanical Engineering, Anyang Institute of Technology, 455000 Anyang, PR China
[b] School of Biological and Chemical Engineering, Chongqing University of Education, 400067 Chongqing, PR China
[c] Hebi Polytechnic, 458000 Hebi, PR China

HIGHLIGHTS

- Porous iron-based metal organic frameworks (NH_2-MIL-101(Fe)) were successfully fabricated via simple one-pot hypothermal reaction.
- The as-synthesized NH_2-MIL-101(Fe) has high surface area and outstanding stability ability.
- Remarkable azo dye degradation performance of NH_2-MIL-101(Fe) in wastewater was obtained.

GRAPHICAL ABSTRACT

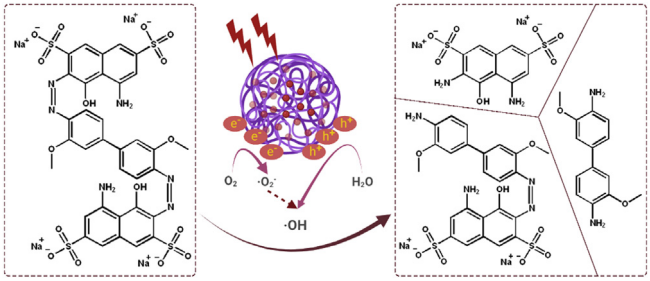

ARTICLE INFO

Keywords:
NH_2-MIL-101(Fe)
Azo dye
Wastewater treatment
Hydroxyl radical

ABSTRACT

The porous iron-based metal organic frameworks (NH_2-MIL-101(Fe)), which consists of 2-amino benzene dicarboxylic acid (H_2BDC-NH_2) and ferrous ions were synthesized through one-step hydrothermal method. The surface area and pore volume of as-synthesized NH_2-MIL-101(Fe) were 66.48 m^2/g and 0.09 cm^3/g, respectively. The excellent photocatalytic performance endows NH_2-MIL-101(Fe) to generate hydroxyl radical (•OH), which then acting as efficiently active sites for azo dye degradation in wastewater. Meanwhile, the outstanding stability ability of NH_2-MIL-101(Fe) indicates the potential candidate for wastewater treatment.

1. Introduction

Azo dyes, defined as the compounds which own a diazotized amine link to a phenol or an amine and contain one or more azo linkages (Chung 2016), are broadly employed in the field of pharmaceutical, textile, leather, and food industries (Yamjala et al., 2016; Clonfero et al., 1990; Brü schweiler and Merlot, 2017; Gič evi ć et al., 2020). Especially in textile industry around the world, azo dyes occupy about 60–70% market share for all inorganic dyes manufacture (Foster et al., 2019). It also means that azo dyes are the main chemical contaminants in waste water of textile industry (Mahmoodi et al., 2012). Previous studies have demonstrated that azo dyes are mutagenic, toxic and potential carcinogens (Alves de Lima et al., 2007; de Aragão Umbuzeiro et al., 2005; Gottlieb et al., 2003). Once azo dyes are systemically absorbed, they will be metabolized by liver cells to generate hazardous aromatic amines (Pinheiro et al., 2004). Therefore, it is of great significance and necessity to degrade the azo dyes in waste water.

In recent years, various chemical, physical and biological strategies have been employed to purify the wastewater, including electrocatalysis, electrochemical destruction, sedimentation, membrane

* Corresponding author.
E-mail address: wangyue@cque.edu.cn (Y. Wang).

https://doi.org/10.1016/j.heliyon.2022.e09942
Received 23 March 2022; Received in revised form 25 May 2022; Accepted 8 July 2022

separation, filtration, and microbial degradation (Paździor et al., 2019; Zhang and Chen, 2020; Ahmed et al., 2021). However, most of these procedures fail to apply in real industry because of the high cost or poor removal efficacy. Different from biological and mechanical techniques, chemical wastewater treatment can enable the treated water to enter the water body for an optimized efficiency. Meanwhile, chemical treatment strategies like chemical oxidation technique have emerged as green method by transfer pollutants into harmless products via chemical catalysts. For example, advanced oxidation processes as an advanced oxidation approach, has been evolved for simultaneous treating wastewater via reactive radicals (Cuerda-Correa et al., 2020). Previous study demonstrated that the intensity of UV photocatalysis was three folds for total carbon content reduction in terms of energy (Halomoan et al., 2022; Yulizar et al., 2021). Photocatalysis strategy owns several advantages including low cost, reusable catalyst, operating under ambient temperature and pressure (Mahmoodi and Saffar-Dastgerdi, 2020). Therefore, developing a safe, high-efficient, green photocatalyst becomes the most important solution for practical application.

Herein, in this study, we report a porous iron-based metal organic frameworks (NH_2-MIL-101(Fe)), which consists of 2-amino benzene dicarboxylic acid (H_2BDC-NH_2) and ferrous ions for photocatalysis of azo dyes in wastewater treatment. The surface area, pore volume, and excellent photocatalytic performance of as-synthesized NH_2-MIL-101(Fe) were systematically examined, respectively. The NH_2-MIL-101(Fe) can effectively generate hydroxyl radical (•OH) under UV irradiation, which then acting as efficiently active sites for azo dye degradation in wastewater. The outstanding stability ability of NH_2-MIL-101(Fe) indicates the potential candidate for wastewater treatment.

2. Materials and experimental methods

2.1. Chemicals and materials

2-amino benzene dicarboxylic acid (NH_2–H_2DBC) and direct turquoise blue (DTB5B) were purchased from Aladdin (Shanghai, China). Anhydrous ferric chloride ($FeCl_3$), N, N-Dimethylformamide (DMF), hydrogen peroxide, and dimethyl sulfoxide (DMSO) were brought from Sinopharm (Beijing, China). TMB single-component substrate solution was obtained from Solarbio life science (Beijing, China). Deionized water and anhydrous ethanol were purchased from Beijing Chemical Industry Group Co., Ltd (Beijing, China). All chemicals were used without any purify.

2.2. Characterizations

Scanning electron microscopy (SEM, SU-8010, Hitachi) and Transmission electron microscopy (TEM, HT-7700, Hitachi) were employed to explore the morphologies of as-synthesized NH_2-MIL-101(Fe). X-ray diffraction patterns of NH_2-MIL-101(Fe) was examined by X-ray diffractometer (D/max-2550, Rigku). TGA-DSC curve for NH_2-MIL-101(Fe) was obtained by thermogravimetric analysis-differential scanning calorimetry (TGA-DSC) (Q5000IR, TA INSTRUMENTS). Fourier transform infrared spectroscopy (FTIR) (X70, NETZSCH) was used to analyze the FTIR spectrum curve of NH_2-MIL-101(Fe). X-ray photoelectron spectroscopy (XPS) (ESXALAB250Xi, Thermo Fisher Scientific) was employed to determine the surface chemistry of NH_2-MIL-101(Fe). Nitrogen adsorption-desorption isotherms and BJH pore size distribution was determined by thermal desorption aerosol gas chromatography (7890B, Agilent).

2.3. Preparation of NH_2-MIL-101(Fe)

NH_2-MIL-101(Fe) was synthesized via a hydrothermal reaction strategy. In detail, 1.242 mmol NH_2–H_2DBC was added in 7.5 mL DMF to form the A solution. Then 2.497 mmol $FeCl_3$ was dissolved in 7.5 mL DMF to form the B solution. Both A and B solution were mixed and transferred into a 30 mL autoclave. After treatment in a 110 °C oven for 24 h, the NH_2-MIL-101(Fe) was obtained by washing with deionized water twice.

2.4. Photocatalytic performance

TMB single-component substrate solution was used to measure the photocatalytic performance of NH_2-MIL-101(Fe) under 300 W Xenon lamp ($\lambda > 300$ nm). In detail, 5 μL TMB (20 mg/mL in DMSO) solution and 1 mL 100 μM H_2O_2 solution were mixed for further analysis. Then different concentration of Fe-MOF aqueous solution was added to make final concentration of 0.125, 0.25, 0.5, 1.0, 2.0 mg/mL. After complete dissolution, the mixture was exposed under 300 W Xenon lamp ($\lambda > 300$ nm) to 10 min. The mixture was centrifugated and supernatant was used for fluorescence detection at about 426 nm (Excitation 312 nm).

2.5. Photocatalytic azo degradation performance

The photocatalytic azo degradation performance of as-prepared NH_2-MIL-101(Fe) was determined by the degradation of direct turquoise blue (DTB5B). Typically, 20 μg/mL DTB5T and various concentration of NH_2-MIL-101(Fe) (0, 15, 31, 62, 125, 250 μg/mL) were mixed in a total 3 mL mixture. Then the mixture was exposed under a 300 W Xenon lamp ($\lambda > 300$ nm). At designed time intervals, 100 μL of the reaction system was withdrawn and centrifugated. The progress of DTB5B degradation was measured by monitoring the UV-vis absorption at 600 nm of supernatant.

3. Results and discussion

3.1. Characterization of nanomaterials

Figure 1a demonstrates the components of as-synthesized NH_2-MIL-101(Fe), in which NH_2–H_2DBC coordinates with ferric ion to form the assemble spherical structure. The morphology of as-synthesized NH_2-MIL-101(Fe) was determined by both SEM and TEM, which are shown in Figure 1. SEM image (Figure 1b) presents the agglutinate spherical structure of NH_2-MIL-101(Fe) and the size distribution is homogeneous. The agglutinate state of NH_2-MIL-101(Fe) is confirmed by the TEM image (Figure 1c), which further demonstrates the unconsolidated and porous structure (Senthil Raja et al., 2019). It can be concluded from the TEM image that the average diameter of as-synthesized NH_2-MIL-101(Fe) is about 50 nm. In order to measure the structure stability, as-synthesized NH_2-MIL-101(Fe) was kept in room temperature for 2 months and there are not significant morphologic changes (Figure 2), indicating the long-term stability. It is well-known that the interaction between ferric ions and NH_2–H_2DBC is coordination bonding and the ferric ions are four-coordinate. Therefore, it is easy to form the porous structure via one ferric ion coordinating with three NH_2–H_2DBC molecules. The X-ray diffraction pattern of NH_2-MIL-101(Fe) presents the crystal structure of as-synthesized sample (Figure 1d). The TGA curve in Figure 1e exhibits that as-synthesized NH_2-MIL-101(Fe) is unstable under higher 360 °C environment and a quickly chemical damage happens when temperature is above 360 °C. Luckily, NH_2-MIL-101(Fe) is structural stable under 100 °C condition, which will benefit the wastewater treatment in ambient environment.

3.2. FTIR analysis

In order to evaluate the composition of NH_2-MIL-101(Fe), FTIR spectroscopic measurement was adopted for analysis and the results is shown in Figure 3. Peak at about 3400 cm^{-1} presents the characteristic vibration bands of the –NH_2 group in NH_2–H_2BDC (Liu et al., 2017). Meanwhile, vibration bands of about 2900 cm^{-1} is the contribution of the methylene in the benzene ring of NH_2–H_2BDC. Peaks at about 1378 cm^{-1} and 1623 cm^{-1} are associated with the C–O vibration (Boontongto and Burakham, 2019). Furthermore, Fe–O contributes the peak at around

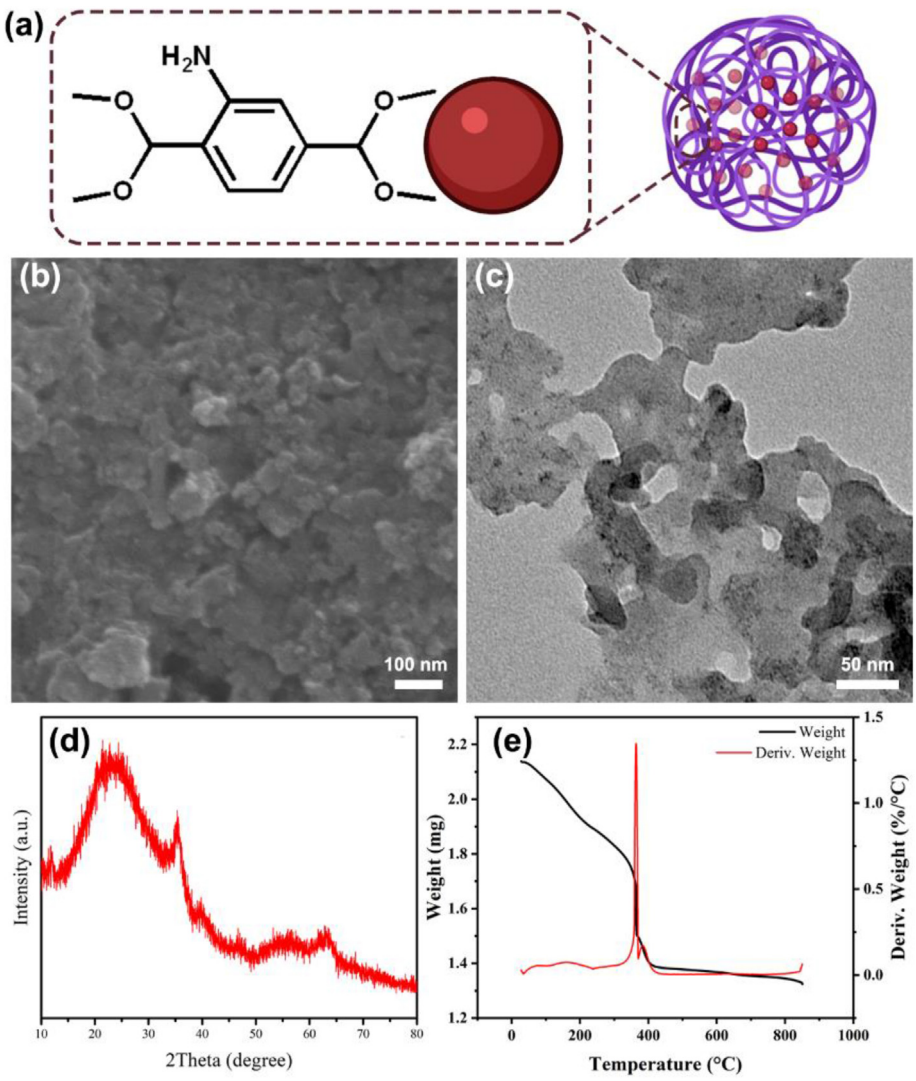

Figure 1. Basic characterization of NH_2-MIL-101(Fe). (a) Schematic illustration of the formation mechanism of NH_2-MIL-101(Fe). (b) The SEM image and (c) TEM image of NH_2-MIL-101(Fe). (d) The X-ray diffraction pattern of NH_2-MIL-101(Fe). (e) The TGA curve of NH_2-MIL-101(Fe) from room temperature to 850 °C.

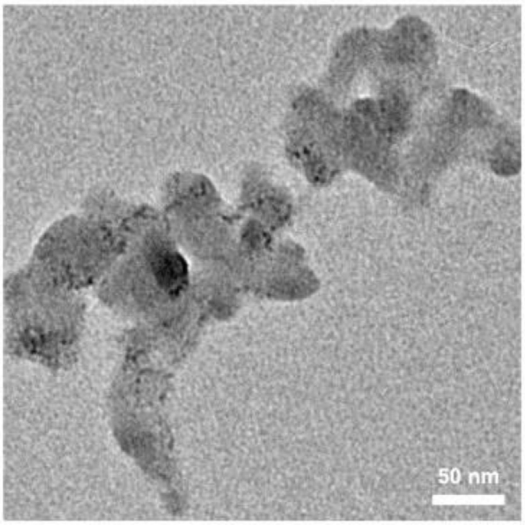

Figure 2. The TEM image of NH_2-MIL-101(Fe) after keeping in ambient temperature for 2 months.

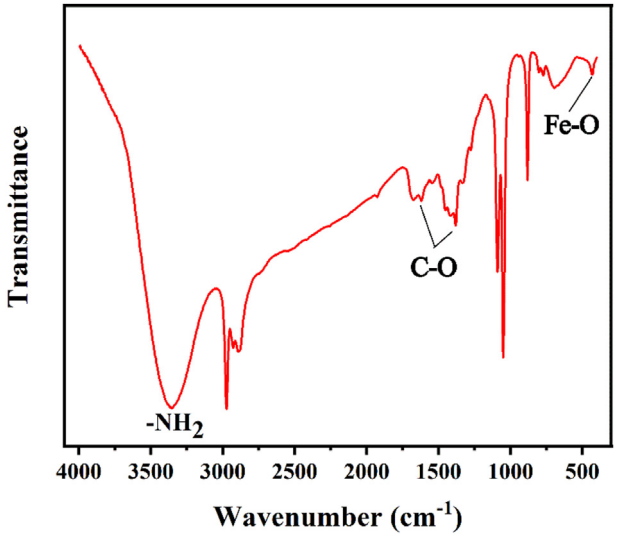

Figure 3. The FTIR spectra curve for NH_2-MIL-101(Fe).

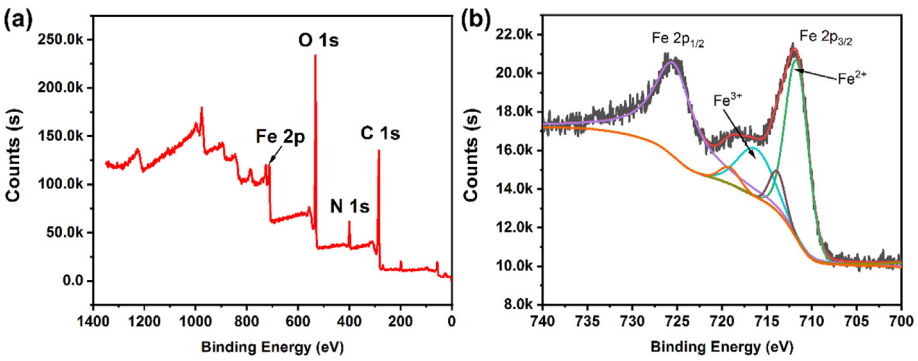

Figure 4. (a) XPS full spectra and (b) high-resolution Fe 2p for NH_2-MIL-101(Fe).

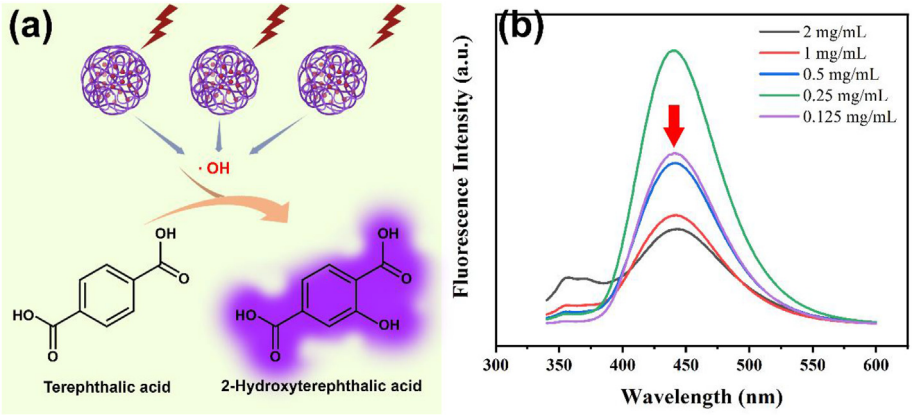

Figure 5. (a) Schematical illustration of peroxidase activity of NH_2-MIL-101(Fe) and (b) fluorescent absorbance of terephthalic acid after treated with different concentration of NH_2-MIL-101(Fe).

431 cm^{-1}. All of these results demonstrated that the coordination bond to Fe^{2+} ions of NH_2–H_2BDC molecular is carbonyl group (C=O), not amine group (NH_2).

3.3. XPS analysis

X-ray photoelectron spectroscopy (XPS) measurement is employed to analyze the surface composition and also the chemical states of elements in NH_2-MIL-101(Fe). The survey curve (Figure 4a) from 0 eV to about 1350 eV clearly shows the binding energy of around 285.4 eV, 400.1 eV, 533.4 eV, and 712.4 eV contribute to the C 1s, N 1s, O 1s, and Fe 2p, respectively. Further analysis of the Fe 2p high-resolution spectrum aids to explore the specific chemical state of Fe in NH_2-MIL-101(Fe) and the results are shown in Figure 4b the Fe 2p1/2 and Fe 2p3/2 binding energy locates around 725.7 eV and 711.9 eV, respectively. Meanwhile, the intensity of integral of peak separation clearly reveals the main valence state of Fe in NH_2-MIL-101(Fe) is divalent, which is agreement with four-coordination structure of NH_2-MIL-101(Fe). (Zhang et al., 2016; Capková et al., 2020).

3.4. Photocatalytic performance

Terephthalic acid (THA) is "para-carboxy benzoate" and there is only one monohydroxylate isomer because of the symmetry structure. The 2-monohydroxyterephthalic acid (THA-OH), which is the reaction product of THA with hydroxyl radical, is intensely fluorescent excited by 312 nm light (Barreto et al., 1994). Thus, THA is a sensitive probe to detect the generation of hydroxyl radicals of NH_2-MIL-101(Fe) under light irradiation (Figure 5a). The fluorescent curve of generated THA-OH (Figure 5b) demonstrates that after NH_2-MIL-101(Fe) and 300 W Xenon lamp ($\lambda > 300$ nm) treatment a significant fluorescence absorbance was detected at around 426 nm, which is the excitation wavelength of produced THA-OH from THA. This phenomenon indicates NH_2-MIL-101(Fe) could effectively produce hydroxyl radials (·OH) after irradiation. Besides, with the concentration increase of NH_2-MIL-101(Fe) in reaction system under same time irradiation, the fluorescence intensity enhances firstly and then gradually decrease, indicating the photocatalytic activity is concentration-dependent (Figure 5b). Previous studies have demonstrated that ligand-to-cluster charge transfer (LCCT) mechanism contributes to the photocatalytic performance of amine-functionalized metal (M) containing metal organic frameworks

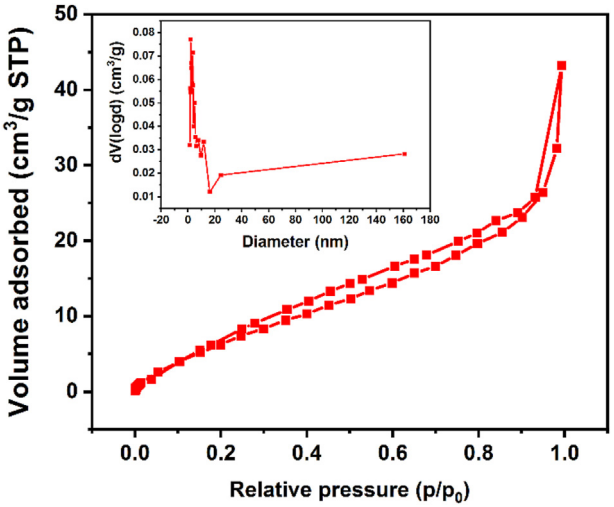

Figure 6. N_2 adsorption-desorption isotherm and pore size (insert figure) of NH_2-MIL-101(Fe).

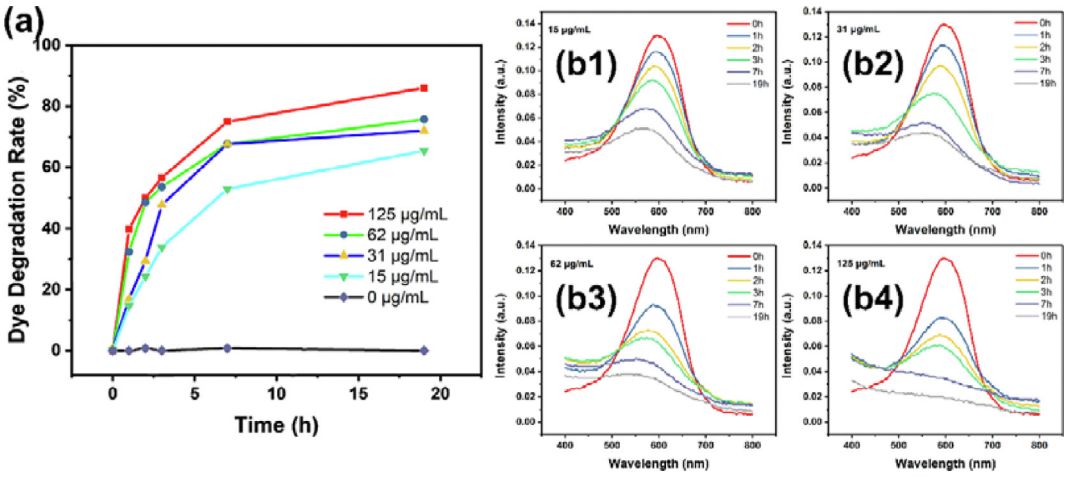

Figure 7. (a) Photocatalytic degradation efficiency of DTB5B dyes treated with NH_2-MIL-101(Fe) (15, 31, 62, 125 μg/mL) for different time under 300 W Xenon lamp (b1-b4) The absorption curve of photocatalytic degradation system treated with various concentration of NH_2-MIL-101(Fe).

(Zhang et al., 2016; Li et al., 2002). Specifically, the NH_2 functionality of NH_2–H_2DBC molecular in NH_2-MIL-101(Fe) effectively absorb the visible light, and then the NH_2–H_2DBC will transfer photoelectrons to Fe–O clusters. After Fe–O clusters are excited, the charge carriers will be delivered to surface of catalyst to form the final ·OH.

3.5. Adsorption behaviors

The porous structure of prepared NH_2-MIL-101(Fe) indicates an efficient adsorption performance in waste water. Therefore, the porosity was measured using N_2 adsorption at 77 K and the adsorption/desorption isotherms are shown in Figure 6. The results demonstrate that NH_2-MIL-101(Fe) exhibits a surface area of 66.5 m^2/g with pore volume of 0.082 cm^3/g. Further testing reveals the pore diameter of NH_2-MIL-101(Fe) is about 2.1 nm. According to the classification of IUPAC, the adsorption-desorption isotherm of NH_2-MIL-101(Fe) is classified as type V (Alothman, 2012).

3.6. Photocatalytic azo degradation performance

In order to evaluate the photocatalytic activity of NH_2-MIL-101(Fe), the commercial direct turquoise blue (DTB5B) dye was chosen as the sample. The concentration of DTB5B aqueous solution was 20 mg/L and the concentration of photocatalyst varies from 15 to 125 mg/L Figure 7a presents the total degradation conditions of DTB5B photocatalyzed by NH_2-MIL-101(Fe) under continuous irradiation of visible light ($\lambda > 300$ nm). Compared with control group without catalyst, low concentration of 15 mg/L NH_2-MIL-101(Fe) can effectively degrade 65.7 % DTB5B during 19 h (Figure 7b1). Meanwhile, the kinetic results exhibit that a better degradation efficiency can be obtained via increasing either photocatalyst concentration or photo-irradiation time. 86% of DTB5B was degraded within 19 h when catalyzed by 125 mg/L NH_2-MIL-101(Fe), which is highly effective than modified TiO_2 catalysts (Liu et al., 2017). Kinetics measurement demonstrates the first order degradation performance of NH_2-MIL-101(Fe) (Figure 8). Furthermore, the photocatalytic stability and reusability were explored via five-cycle experiments and the results exhibit there is only 13.7% loss (Figure 9). The highly photocatalyst ability of NH_2-MIL-101(Fe) portends its great potential for azo dye degradation in waste water treatment.

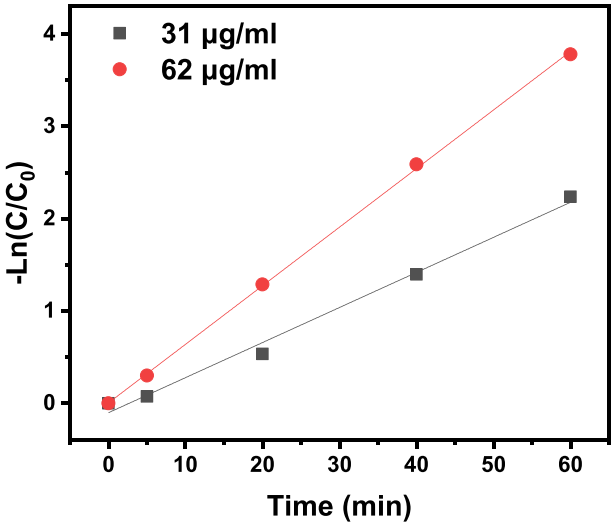

Figure 8. The first order photocatalytic dye degradation at different NH_2-MIL-101(Fe) concentration.

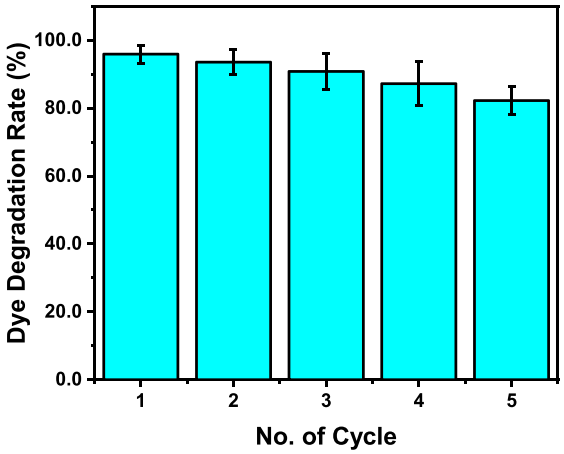

Figure 9. The photocatalytic efficiency of NH_2-MIL-101(Fe) during the five cycles process.

4. Conclusions

In summary, the porous NH_2-MIL-101(Fe) were synthesized through a simple one-step hydrothermal method. The as-synthesized NH_2-MIL-101(Fe) reveals high surface area and pore volume of 66.48 m^2/g and 0.09 cm^3/g, respectively. The porous structure and excellent photocatalytic performance enable NH_2-MIL-101(Fe) degrade DTB5B dye in waste water

efficiently with low concentration. The excellent photocatalytic performance is contributed by generated hydroxyl radical (•OH) under photo-irradiation, which then acting as efficiently active sites for azo dye degradation in wastewater. Generally, the outstanding stability ability of NH_2-MIL-101(Fe) indicates the potential candidate for wastewater treatment. Admittedly, as a catalyst, it is vital to design and explore the recovery and recycling performances of NH_2-MIL-101(Fe) in the near future.

Declarations

Author contribution statement

Xuezhong Li: Performed the experiments; Analyzed and interpreted the data; Wrote the paper.

Yue Wang: Conceived and designed the experiments.

Qi Guo: Contributed reagents, materials, analysis tools or data.

Funding statement

This work was supported by the Doctoral Initial Scientific Research Fund of Anyang Institute of Technology (BSJ2019017), the Science and Technology Research Program of Chongqing Municipal Education Commission (KJQN202101610), the Natural Science Foundation of Chongqing (cstc2019jcyj-msxm0851) and the Scientific Research Project of Chongqing University of Education (KY201906B).

Data availability statement

Data included in article/supplementary material/referenced in article.

Declaration of interests statement

The authors declare no conflict of interest.

Additional information

No additional information is available for this paper.

References

Ahmed, S.F., Mofijur, M., Nuzhat, S., Chowdhury, A.T., Rafa, N., Uddin, Md.A., Inayat, A., Mahlia, T.M.I., Ong, H.C., Chia, W.Y., Show, P.L., 2021. Recent developments in physical, biological, chemical, and hybrid treatment techniques for removing emerging contaminants from wastewater. J. Hazard Mater. 416, 125912.

Alothman, Z., 2012. A review: fundamental aspects of silicate mesoporous materials. Materials 5, 2874–2902.

Alves de Lima, R.O., Bazo, A.P., Salvadori, D.M.F., Rech, C.M., de Palma Oliveira, D., de Aragão Umbuzeiro, G., 2007. Mutagenic and carcinogenic potential of a textile azo dye processing plant effluent that impacts a drinking water source. Mutat. Res. Toxicol. Environ. Mutagen. 626, 53–60.

Barreto, J.C., Smith, G.S., Strobel, N.H.P., McQuillin, P.A., Miller, T.A., 1994. Terephthalic acid: a dosimeter for the detection of hydroxyl radicals in vitro. Life Sci. 56, 89–96.

Boontongto, T., Burakham, R., 2019. Evaluation of metal-organic framework NH2-MIL-101(Fe) as an efficient sorbent for dispersive micro-solid phase extraction of phenolic pollutants in environmental water samples. Heliyon 5, e02848.

Brüschweiler, B.J., Merlot, C., 2017. Azo dyes in clothing textiles can be cleaved into a series of mutagenic aromatic amines which are not regulated yet. Regul. Toxicol. Pharmacol. 88, 214–226.

Capková, D., Almási, M., Kazda, T., Čech, O., Király, N., Čudek, P., Fedorková, A.S., Hornebecq, V., 2020. Metal-organic framework MIL-101(Fe)–NH2 as an efficient host for sulphur storage in long-cycle Li–S batteries. Electrochim. Acta 354, 136640.

Chung, K.T., 2016. Azo dyes and human health: a review. J. Environ. Sci. Health, Part A C. 34, 233–261.

Clonfero, E., Venier, P., Granella, M., Levis, A.G., 1990. Leather azo dyes: mutagenic and carcinogenic risks. Med. Lav. 81, 222–229.

Cuerda-Correa, E.M., Alexandre-Franco, M.F., Fernández-González, C., 2020. Advanced oxidation processes for the removal of antibiotics from water. An overview. Water 12, 102.

de Aragão Umbuzeiro, G., Freeman, H.S., Warren, S.H., de Oliveira, D.P., Terao, Y., Watanabe, T., Claxton, L.D., 2005. The contribution of azo dyes to the mutagenic activity of the Cristais River. Chemosphere 60, 55–64.

Foster, S.L., Estoque, K., Voecks, M., Rentz, N., Greenlee, L.F., 2019. Removal of synthetic azo dye using bimetallic nickel-iron nanoparticles. J. Nanomater. 2019, 1–12.

Gottlieb, A., Shaw, C., Smith, A., Wheatley, A., Forsythe, S., 2003. The toxicity of textile reactive azo dyes after hydrolysis and decolourisation. J. Biotechnol. 101, 49–56.

Gičević, L., Hindija, A., Karačić, 2020. Toxicity of Azo Dyes in Pharmaceutical Industry. CMBEBIH 2019, 2020. Springer International Publishing, Cham, pp. 581–587.

Halomoan, Y., Yulizar, R.M., Surya, D.O.B., 2022. Apriandanu, Facile preparation of CuO-Gd2Ti2O7 using Acmella uligi$_n$os$_a$ $_l$eaf extract for photocatalytic degradation of malachite green. Mater. Res. Bull. 150, 111726.

Li, W.Q., Wang, Y.X., Chen, J.Q., Hou, N.N., Li, Y.M., Liu, X.C., Ding, R.R., Zhou, G.N., Li, Q., Zhou, X.G., Mu, Y., 2002. Boosting photo-Fenton process enabled by ligand-to-cluster charge transfer excitations in iron-based metal organic framework. Appl. Catal. B Environ. 302, 120882.

Liu, M., Liu, Y., Zhang, D., Pan, J., Liu, B., Ouyang, S., 2017. Facile fabrication of H_2BDC-NH_2 modified anatase TiO_2 for effective photocatalytic degradation of azo dyes. Can. J. Chem. Eng. 95, 922–930.

Mahmoodi, N.M., Bashiri, M.S., Moeen, J., 2012. Synthesis of nickel–zinc ferrite magnetic nanoparticle and dye degradation using photocatalytic ozonation. Mater. Res. Bull. 47, 4403–4408.

Mahmoodi, N.M., Saffar-Dastgerdi, M.H., 2020. Clean Laccase immobilized nanobiocatalysts (graphene oxide - zeolite nanocomposites): from production to detailed biocatalytic degradation of organic pollutant. Appl. Catal. B Environ. 268, 118443.

Paździor, K., Bilińska, L., Ledakowicz, S., 2019. A review of the existing and emerging technologies in the combination of AOPs and biological processes in industrial textile wastewater treatment. Chem. Eng. J. 376, 120597.

Pinheiro, H.M., Touraud, E., Thomas, O., 2004. Aromatic amines from azo dye reduction: status review with emphasis on direct UV spectrophotometric detection in textile industry wastewaters. Dyes Pigments 61, 121–139.

Senthil Raja, D., Lin, H.W., Lu, S.Y., 2019. Synergistically well-mixed MOFs grown on nickel foam as highly efficient durable bifunctional electrocatalysts for overall water splitting at high current densities. Nano Energy 57, 1–13.

Yamjala, K., Nainar, M.S., Ramisetti, N.R., 2016. Methods for the analysis of azo dyes employed in food industry – a review. Food Chem. 192, 813–824.

Yulizar, Y., Eprasatya, A., Bagus Apriandanu, D.O., Yunarti, R.T., 2021. Facile synthesis of ZnO/$GdCoO_3$ nanocomposites, characterization and their photocatalytic activity under visible light illumination. Vacuum 183 (2021), 109821.

Zhang, Z., Li, X., Liu, B., Zhao, Q., Chen, G., 2016. Hexagonal microspindle of NH2-MIL-101(Fe) metal–organic frameworks with visible-light-induced photocatalytic activity for the degradation of toluene. RSC Adv. 6, 4289–4295.

Zhang, Z., Chen, Y., 2020. Effects of microplastics on wastewater and sewage sludge treatment and their removal: a review. Chem. Eng. J. 382, 122955.